TRENDS IN SCIENCES 2026; 23(2): 11438
https://doi.org/10.48048/tis.2026.11438 RESEARCH ARTICLE

In Vitro Antiviral Activity and Molecular Docking Analysis of Dihydropyrimidinone, Chromene and Chalcone Derivatives Against SARS-CoV-2

Dinar Adriaty[1,4], Hery Suwito[2,3,*], Ni Nyoman Tri Puspaningsih[2,3], Adita Ayu Permanasari[4], Aldise Mareta Nastri[4], Kazufumi Shimizu[4,5]

[1]*Doctoral Program of Mathematics and Natural Sciences, Faculty of Science and Technology, Universitas Airlangga, MERR-C Mulyorejo, East Java 60115, Indonesia*
[2]*Department of Chemistry, Faculty of Science and Technology, Universitas Airlangga, MERR-C Mulyorejo, Surabaya East Java 60115, Indonesia*
[3]*UCoE Research Center for Bio-Molecule Engineering, (BIOME), Universitas Airlangga, MERR-C Mulyorejo, East Java 60115, Indonesia*
[4]*Institute of Tropical Disease, Indonesia-Japan Collaborative Research Center for Emerging and Re-Emerging Infectious Diseases, Universitas Airlangga, MERR-C Mulyorejo, East Java 60115, Indonesia*
[5]*Center for Infectious Diseases, Graduate School of Medicine, Kobe University, Kobe 657-8501, Japan*

([*]Corresponding author's e-mail: hery-s@fst.unair.ac.id)

Received: 30 July 2025, Revised: 9 September 2025, Accepted: 19 September 2025, Published: 1 November 2025

Abstract

To identify and develop effective antiviral agents against SARS-CoV-2, research is ongoing in the field of drug discovery. Heterocyclic compounds such as Chalcone, Chromene, and Dihydropyrimidinone (DHPM) derivatives are of particular interest because of their structural diversity, easily synthesized and broad pharmacological activities, including antiviral effects. Therefore, we investigated the potential of these derivatives against SARS-CoV-2 using cell-based assays, supported by *in silico* studies. Ten synthetic compounds, consist of 4 DHPMs, 2 chromenes, and 4 chalcones were tested for cytotoxicity and antiviral activity in Vero cells infected with a locally isolated SARS-CoV-2 strain (Clade GH, GISAID: EPI_ISL_529965), using a phenotypic screening approach. Moreover, *in silico* analyses were performed to predict their drug-likeness, including absorption, distribution, metabolism, and excretion properties, using SwissADME. Molecular docking was conducted to evaluate the binding affinity and interactions of compounds with the SARS-CoV-2 main protease (Mpro). Among the tested compounds, S-10 (chromene derivative) and S-12 (DHPM derivative) demonstrated exhibited significant antiviral activity compared to the other tested derivatives ($p < 0.05$), with IC_{50} values of 8.52 ± 0.28 µM and 6.19 ± 0.41 µM, and selectivity index (SI) of 158.8 and 309.7, respectively, indicating strong efficacy and high safety margins. *In silico* ADME suggested favorable drug-likeness profiles without major toxicity alerts. Molecular docking further revealed that both compounds established stable interactions with the SARS-CoV-2 main protease (Mpro), particularly at the catalytic residues His-41 and Cys-145, supporting their *in vitro* activity. These results suggest their potential as lead compounds for further drug development, supporting the use of integrated phenotypic and computational approaches in the discovery of region-specific antiviral agents.

Keywords: Antiviral, Chalcone, Chromene, Dihydropyrimidinone, SARS-CoV-2

Introduction

SARS-CoV-2 is an infectious disease caused by a novel coronavirus that was first identified in December 2019 in Wuhan, China. Notably, its rapid global spread prompted the World Health Organization to declare it a global pandemic [1,2]. SARS-CoV-2 belongs to the family *Coronaviridae* and is characterized by a diameter

of 60 - 140 nm; 9 - 12 nm spike proteins, which give it a solar corona-like appearance [3]. Vaccines are available and have significantly reduced morbidity and mortality. However, their long-term effectiveness is challenged by the frequent emergence of new viral variants, particularly those with mutations in the spike protein, a primary target for neutralizing antibodies [4]. Such mutations may compromise vaccine performance and highlight the need for effective antiviral therapies.

Although several drugs, such as remdesivir have been approved by Food and Drug Administration (FDA) or have received Emergency Use Authorizations (EUAs) such as lopinavir, ribavirin, ritonavir-boosted nirmatrelvir (paxlovid), chloroquine and ivermectin as antiparasitic agents, and the antibiotic azithromycin, which have been employed individually or in combination as analog therapies for the treatment of SARS-CoV-2, most of them are repurposed drugs originally developed for other diseases. Some of these drugs, also remains limited by issues such as high cost, limited availability in some regions, and administration requirements (e.g., intravenous remdesivir) [5,6]. The continuous emergence of viral variants further threatens the durability of these therapies. Therefore, discovering novel compounds with simpler structures, potential oral bioavailability, and affordable synthesis is essential, particularly in low-resource settings. Such efforts are aligned with the United Nations Sustainable Development Goals (SDGs), especially Goal 3 (Good Health and Well-Being) and Goal 10 (Reduced Inequalities), by promoting equitable access to effective and sustainable treatments [7].

To address these limitations, phenotypic screening has re-emerged as a valuable strategy. Phenotypic screening is an approach in drug development that focuses on observing and understanding phenotypic changes that occur at the cellular, tissue, or whole organism level in response to certain substances or chemical compounds [8]. Unlike target-based screening, which requires prior knowledge of specific molecular targets such as enzymes or receptors and may overlook compounds with broader or multi-target effects [9], phenotypic screening approach directly evaluates the biological effects of compounds in infected cells. This approach captures complex cellular interactions and increases the likelihood of identifying novel scaffolds with antiviral activity, even when their mechanisms of action are not fully understood. By starting from observed cellular responses, phenotypic screening accelerates the identification of active molecules while minimizing the risk of missing compounds with multi-target or indirect effects [10]. After screening candidate compounds on cells and microorganisms, potential compounds are further studied for their pharmacokinetic properties, such as absorption, distribution, metabolism, and excretion (ADME) [11]. Importantly, while phenotypic screening serves as the primary strategy, complementary target-based analyses such as molecular docking were employed to provide molecular insights [12]. This integration enables a better understanding of the observed phenotypic effects and offers preliminary explanations of the possible modes of action of the candidate compounds.

Heterocyclic compounds such as dihydropyrimidinones (DHPMs) [13,14], chalcones [15], and chromenes [16] represent promising scaffolds for this purpose. They are easily synthesized, structurally diverse, and they exhibit broad pharmacological activities including antiviral, antibacterial, antiparasitic, antifungal, anti-inflammatory, and anticancer properties [17].

DHPM and pyrimidine derivatives are recognized as nucleobase analogs with activity against viral polymerases and proteases [18]. Chromenes, structurally related to flavonoids, have been linked to antiviral and anti-inflammatory effects [19], while chalcones, with their reactive enone system, display broad-spectrum, multi-target antiviral and immunomodulatory potential [20]. Both chalcone and chromene derivatives have shown consistent activity against RNA viruses, including HIV, HCV, and influenza. Their versatility makes them attractive candidates for drug discovery programs targeting emerging viral infections.

However, despite these interesting findings, studies exploring their potential against SARS-CoV-2 remain limited. Therefore, this study aimed to conduct a preliminary evaluation of chalcone, chromene, and DHPM derivatives against SARS-CoV-2. To achieve this, a phenotypic screening approach was employed using a local isolated viral strain, assessing cytotoxicity and antiviral activity. This was followed by *in silico* ADME profiling to predict pharmacokinetics and molecular docking, including grid score and docking

pose/pharmacophore score, to explore possible mechanisms of action targeting the main protease enzyme of SARS-CoV-2. As an early-stage investigation, this comprehensive approach is expected to facilitate the identification of promising lead compounds for further development as anti-SARS-CoV-2 therapeutics.

Materials and methods

Materials

All chemical reagents, including 100% dimethyl sulfoxide (DMSO), [3-(4,5-dimethylthiazol-2yl)-5(3-carboxymethoxyphenyl)-2-(4-sulfophenyl0-2H-terazolium] (MTT), phosphate buffer saline (PBS), and 1% penicillin-streptomycin, were obtained from Sigma-Aldrich, USA. Sterilization was performed using 0.22 µm membrane filters (OMNIPORE, Millipore). Cell culture was performed using Dulbecco's Modified Eagle Medium (DMEM) with glucose (Biowest), supplemented with 5% Fetal Bovine Serum (FBS) from Biowest, and Trypsin TPCK (Worthington Biochemical Corporation, USA). RNA extraction was performed using the RNeasy Kit (QIAGEN, USA), and qRT-PCR was conducted using the STANDARD™ M nCoV Real-Time Detection Kit (SD Biosensor Inc., Korea) [21]. Ten synthetic compounds (4 DHPMs, 2 chromenes, and 4 chalcones) were sourced from BIOME, Universitas Airlangga. Vero ATCC CCL-81 (https://www.atcc.org/products/ccl-81) cells were provided by the Center of Infectious Diseases, Kobe University, Japan, and the SARS-CoV-2 virus isolate (B1.470; GISAID ID: EPI_ISL_529965, Clade GH) [22,23] was obtained from a patient. Reference drug structures were obtained from an online database https://pubchem. ncbi.nlm.nih.gov. The enzyme used for the *in-silico* study was SARS-CoV-2 Main Protease (Mpro) complexed with the non-covalent ligand N-(4-tert-butylphenyl)-N-[(1R)-2 (cyclohexylamino)-2-oxo-1- (pyridin-3-yl)ethyl]-1H-imidazole-4-carboxamide (X77) (PDB ID: 6w63), was retrieved from the RCSB Protein Data Bank (website http://www.rcsb.org/pdb).

Instrumentation

MTT assay was conducted using a Spectroreader Multidetection Microplate Reader Multiskan SkyHigh Photometer (Thermo Fisher Scientific). Virus amplification was performed via qRT-PCR using the Applied Biosystems 7500 Fast system and its accompanying software (Applied Biosystems). GraphPad Prism 8.3.0 software was used to analyze the cytotoxicity and dose-response data. The of ADME properties of the candidate ligands were predicted using the SwissADME tool (https://www.swissadme.ch). Toxicology evaluation was conducted using the Toxicity Estimation Software Tool (T.E.S.T); https://www.epa.gov/comptox-tools/toxicity-estimation-software-tool-test to assess Ames mutagenicity (M) and LD_{50} (mg/kg). Molecular docking analysis was performed using software on 2 operating systems: Windows 10 and Linux. On the Windows system, ChemDraw Professional 15.1, Chimera 1.16, PuTTY (64-bit), WinSCP, and Discovery Studio BIOVIA 2021 2021 v21.1.0.2098 were used to generate 2-dimensional (2D) visual representations of ligand-receptor interactions. On the Linux system, the DOCK 6 program was employed for molecular docking, and Gaussian 16 was utilized for computational calculations.

Cell preparation and virus propagation

Vero cells were cultured in DMEM supplemented with 5% FBS and 1% penicillin-streptomycin and passaged at cell confluency >80%. SARS-CoV-2 was cultured on Vero cells in the presence of 2.5 µg/mL of TPCK-treated trypsin. After centrifugation, the viral supernatant was further propagated on Vero cells to produce a working viral stock. Vero cells used in this study were at passage number 55. Specifically, the stock was prepared by diluting the virus supernatant with 0.2% Bovine Serum Albumin (BSA) in Tris-Glycine-Saline (TGS) in a 2:1 ratio. Notably, viral titer was determined using the 50% tissue culture infectious dose (TCID50) culture method. Briefly, Vero cells were seeded in a 96-well plate at a density of 1×10^4 cells/well for 24 h, followed by dilution at 10 - 1 to 10 - 10. Finally, TCID50 was determined based on the cytopathic effect of the cell infection as well as with qRT-PCR and calculated using the Reed and Munch method [24].

Cell viability assay

Candidate compounds were dissolved in 100% DMSO to prepare 1 M stock solutions. Thereafter, these solutions were filtered through a 0.22 µm membrane under aseptic conditions [25]. Dilutions were prepared

in complete DMEM to achieve the final test concentrations.

Cell viability was assessed using the MTT assay (Sigma-Aldrich) as described by Permanasari *et al*. [26]. Briefly, Vero cells were seeded in 96-well microplates (1×10^4 cells/well) containing 100 µL of DMEM supplemented with 5% FBS and 1% penicillin-streptomycin at 37 °C for 24 h under a 5% CO_2 atmosphere.

Thereafter, Vero cells were treated with the test compounds at dilutions of 1600, 800, 400, 200, 100, and 50 µM in triplicate and incubated for 48 h. Finally, the absorbance was measured at 560 and 750 nm. Cell viability was determined using the following equation [27,28]: % Viable cells = (Treatment Absorbance – Control Medium Absorbance)/(Negative Control Absorbance – Control Medium Absorbance)×100%. Results were obtained using a nonlinear regression equation (analysis 4-parameter logistic model) using GraphPad Prism 8.3.0 software. The results are expressed as the 50% Cytotoxic Dose (CC_{50}).

***In vitro* anti SARS-CoV-2 assay**

Vero cells were seeded in a 96-well plate at a density of 1×10^4 cells/well and incubated for 24 h at 37 °C in a 5% CO_2 atmosphere. After removing the culture medium, the cells were infected with 100 $TCID_{50}$/mL of SARS-CoV-2 virus diluted in DMEM containing 2.5 µg/mL TPCK-treated trypsin, followed by gentle shaking and 1 h incubation [29]. The viral suspension was then removed, and serial concentrations of the test compounds (10, 20, 40, and 80 µM) were added to the infected cells, with each treatment performed in duplicate. The plates were incubated for 72 h under the same conditions, and observations were recorded at 24, 48, and 72 h. Infected Vero cells treated with 0.1% DMSO served as negative controls to establish the baseline level of viral replication. No positive control (e.g., known antiviral drug) was included, as this study was designed as a preliminary phenotypic screening to identify novel compounds with measurable antiviral activities, rather than to directly compare their effects with established agents.

After incubation, RNA was extracted from the supernatants using qRT-PCR. Antiviral activity was quantified using the following formula where $A0$ represents the Average RT-qPCR copy number without a sample, and $A1$ represents the Average RT-qPCR copy number with the sample: % Inhibition = $[(Ao - A_1) / A_0] \times 100\%$ .The IC_{50} value was determined using nonlinear regression analysis (4-parameter logistic model) with GraphPad Prism 8.3.0. One-way ANOVA with Tukey's post hoc test was used to compare IC_{50} values with statistical significance was set at $p < 0.05$ [30]. The selectivity index (SI) values were determined by calculating the ratio of CC_{50} to $IC_{50,}$ and the standard deviation of the SI was calculated using the standard error propagation method. Compounds with an SI >10 were considered potential drug candidates.

RNA extraction and amplification of SARS-CoV-2

SARS-CoV 2 RNA was extracted from fluid samples using the RNeasy kit (Qiagen, Valencia, Calif., USA). Eighty microliters (80 µL) of the culture supernatant were mixed with 320 µL of AVL lysis buffer (Qiagen, Valencia, Calif., USA). After adding 320 µL of 96% ethanol, the samples were filtered using a spin column RNeasy kit to extract the RNA. The extracted RNA was eluted in 60 µL of nuclease-free water.

qRT-PCR was performed to amplify the ORF1ab (RdRp) and E genes using the STANDARD™ M nCoV Real-Time Detection kit (SD Biosensor Inc., Suwon, South Korea). A positive result was reported if ORF1ab or both genes had Ct values within the valid range (<38), and samples with endpoints above the minimum threshold were considered presumptive positives. In contrast, the sample was considered negative if neither target met these criteria. Presumptive positive results were treated as positive owing to their strong indication of SARS-CoV-2 presence [31].

Experimental design and bias control

As this was an initial screening study, formal randomization was not applied. To reduce potential bias, all compounds were anonymized using coded identifiers (e.g., S-1, S-10, C-3, and C-5), and distributed in a balanced, non-systematic order across microplates to minimize the edge effects and positional bias. Cytotoxicity (MTT assay) and antiviral activity (qRT-PCR) were independently assessed by 2 researchers

using instrument-based measurements. Blinding of compound identities further ensured objectivity.

In silico analysis

ADME predictions

Pharmacokinetic analysis of drug similarity properties, including drug-likeness, was performed using the SwissADME program [32,33]. Generally, drug candidate selection is based on ADME properties, according to Lipinski's rule of 5 and the Ghose, Veber, Egan, and Muegge rules [34,35]. Additionally, the Toxicity Estimation Software Tool (T.E.S.T) was used to predict the toxicity and mutagenicity of the compounds, based on various parameters, including LD_{50} and the results of the Ames test for mutagenicity. LD_{50} provides an indication of the toxicity of a substance, with a lower LD_{50} value indicating higher toxicity and a mutagenicity index ≤ 1 indicating no significant increase in mutagenicity. Notably, the closer the total score is to 1, the safer the compound [36,37].

Molecular docking

To prepare SARS-CoV-2 main protease receptor (PDB ID: 6w63), water molecules and non-complex ions were removed, occupancy selection was performed, and charges were added, using ff14SB for the protein and AM1-BCC for non-protein parts [38]. The protein, receptor surface grid and spheres were generated using the molecular docking software Dock-6 [39] and Chimera software. Both programs operate through server usage, necessitating the setup of communication software, such as WinSCP and PuTTY.

Reference drug compounds were sourced from PubChem, and ligand structures in SMILES format were converted into 3D structures using the CACTUS server (https://cactus.nci.nih.gov). Subsequently, the structures were optimized using the PM7 method in Gaussian16, and charges were assigned using Antechamber. Finally, the ligands, receptors, and complexes were saved in the MOL2 format [40].

Docking was performed with a flexible docking approach using DOCK6, and the protocol was validated by re-docking the co-crystallized ligand (X77) onto the receptor. Successful docking validation was confirmed if the ligand's pose matched its original conformation with an RMSD $\leq$ 2 Å, supported by consistent interaction profiles. Here, 'original conformation' refers to the co-crystallized orientation of X77 within the active site of SARS-CoV-2 Mpro (PDB ID: 6w63). Finally, candidate ligands were docked onto the main protease receptor, with selection based on grid scores and generated poses [41].

Results and discussion

In this study, we investigated the antiviral effects of 10 compounds derived from DHPMs, chromene (benzopyrene), and chalcone derivatives will be observed as candidate anti-COVID-19 drugs. DHPMs and Pyrimidinones are heterocyclic compounds synthesized through classic multi-component reactions, such as the Biginelli reaction [42].

Table 1 Drug candidate compounds.

No.	Code	Structure	Derivate	Name of compound (International Union of Pure and Applied Chemistry)
1	C-1	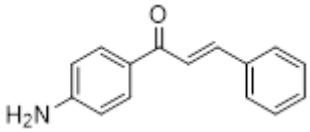	Amino Chalcone	(*E*)-1-(4-aminophenyl)-3-phenylpro-2-en-1-one
2	S-2	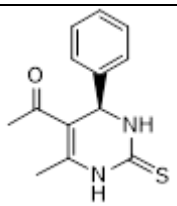	DHPM (DHP-tio)	(*R*)-1-(6-methyl-4-phenyl-2-thioxo-1,2,3,4-tetrahydropyrimidin-5-yl)ethan-1-one

No.	Code	Structure	Derivate	Name of compound (International Union of Pure and Applied Chemistry)
3	S-3	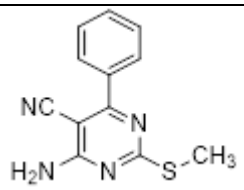	pyrimidine	4-amino-2-(methylthio)-6-phenylpyrimidine-5-carbonitrile
4	S-4	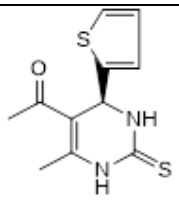	DHPM (DHP-tio)	(*S*)-1-(6-methyl-4-(thiophen-2-yl)-2-thioxo-1,2,3,4-tetrahydropyrimidin-5-yl)ethan-1-one
5	C-5	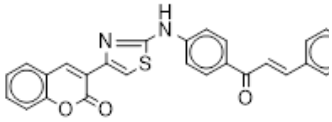	Chalcone Hybrid	3-(2-((4-cinnamoylphenyl)amino)thiazol-4-yl)-2H-chromen-2-one
6	C-6	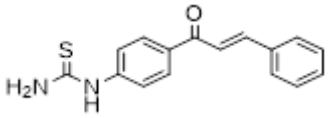	Chalcone- thiourea	1-(4-cinnamoylphenyl)thiourea
7	C-7	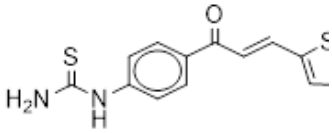	Chalcone- thiourea	(*E*)-1-(4-(3-(thiophen-2-yl)acryloyl)phenyl) thiourea
8	S-10	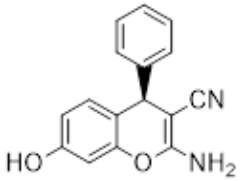	Chromene	(*R*)-2-amino-7-hydroxy-4-phenyl-4*H*-chromene-3-carbonitrile
9	S-11	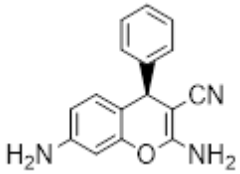	Chromene	(*R*)-2,7-diamino-4-phenyl-4*H*-chromene-3-carbonitrile
10	S-12	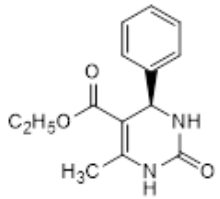	DHPM	ethyl (*R*)-6-methyl-2-oxo-4-phenyl-1,2,3,4-tetrahydropyrimidine-5-carboxylate

In **Table 1**, compound-2 (S-2), compound-3 (S-3), compound-4 (S-4), compound-12 (S-12) are DHPM and pyrimidinones, whereas compound-10 (S-10) and compound-11 (S-11) are chromene. Chromenes also known as benzopyrans, are important compounds that are synthesized for commercial use. Chromenes are characterized by the presence of an oxygen atom in the pyran ring. Chromenes exist in various forms, such as simple chromenes (2H-chromene) and fused chromenes. Recent advances have demonstrated various eco-friendly and efficient strategies for their synthesis, including multicomponent reactions, visible-light photocatalysis, and 1-pot protocols using green catalysts and solvents [43,16].

Chalcones are a group of compounds categorized as flavonoids due to their structural scaffold, which is C6-C3-C6. Chalcone, derivatives can be obtained from natural sources or as synthetic products [44,45]. As shown in **Table 1**, compound-1 (C-1), is an amino chalcone, whereas the other chalcones, including compound-5 (C-5), compound-6 (C-6), and compound-7 (C-7). For Compound C-5, the hybrid combination was achieved by combining active pharmacophores (coumarin and thiazole), whereas the others originated from chalcone thiourea (C-6) and chalcone thiourea executed with thiophene (C-7).

Cytotoxicity of the derivatives

A cell viability assay was performed to assess the cytotoxicity of the 10 compounds, and the results were expressed as CC_{50}. As shown in **Figure 1**, there was a concentration-related reduction in Vero cell viability after treatment with the 10 candidate compounds at concentrations of 50, 100, 200, 400, 800, and 1600 µM

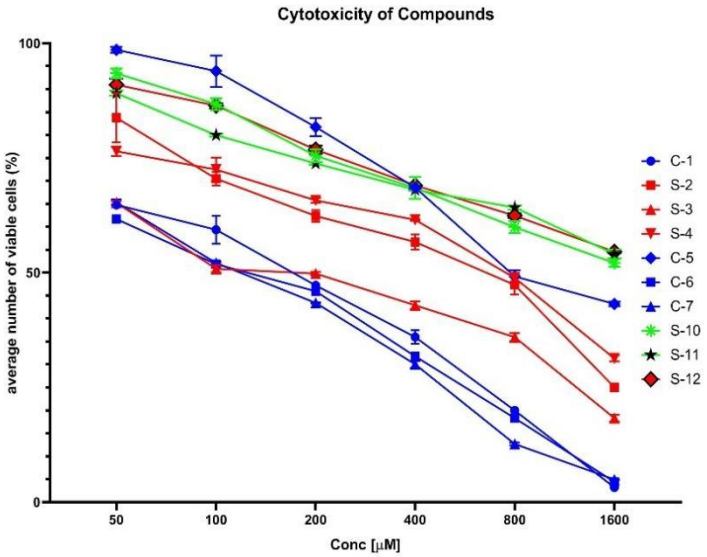

Figure 1 Cytotoxicity of chalcone (C-1, C-5, C-6, C-7), chromene (S-10, S-11), and dihydropyrimidinone (S-2, S-3, S-4, S-12) derivatives in Vero cells at concentrations ranging from 50 to 1600 µM. Data are presented as mean ± SD (each concentration was repeated in triplicate). Color and symbol codes: C-1 (blue-round), S-2 (red-square), S-3 (red-triangle), S-4 (red-invertedtriangle), C-5 (blue-diamond), C-6 (blue-square), C-7 (blue-triangle), S-10 (green-*), S-11 (green-star), and S-12 (red-diamond).

Among them, S-10, S-11 and S-12 demonstrated low cytotoxicity, C-5, S-4, S-2 and S-3 showed moderate cytotoxicity and C-1, C-6 and C-7, exhibited high cytotoxicity.

The CC_{50} values of the compounds are listed in **Table 2**. These values were calculated from dose-response curves using nonlinear regression analysis (4-parameter logistic model) in GraphPad Prism version 8.3.0. Cell viability percentages were plotted against compound concentrations, and the CC_{50} values were derived from the best-fit curves.

Table 2 Cytotoxicity of chalcone, chromene, and DHPM derivatives in Vero cells.

Compounds	CC_{50} (µM, mean ± SD)	Cytotoxicity category*
C-1	147.8 ± 19.78	Strong
S-2	485.5 ± 64.03	Moderate
S-3	166.1 ± 26.43	Strong

Compounds	CC_{50} (μM, mean ± SD)	Cytotoxicity category*
S-4	617.2 ± 85.87	Moderate
C-5	965.4 ± 101.08	Moderate
C-6	117.4 ± 15.07	Strong
C-7	118.8 ± 10.94	Strong
S-10	1596 ± 214.77	Moderate
S-11	2292 ± 356.1	Moderate
S-12	1978 ± 221.52	Moderate

Notes: *>200 μM Moderate Cytotoxicity; 20 - 100 μM Strong Cytotoxicity; 1 - 20 μM Very Strong Cytotoxicity (Indrayanto *et al*. [46]).

Based on a previously established classification system [46], compounds with CC_{50} values of 1 - 20 μM are considered extremely cytotoxic; those with values between 20 and 100 μM are categorized as strongly cytotoxic; and compounds with CC_{50} values ≥200 μM are classified as moderately cytotoxic. Based on this classification, 5 compounds (C-1, C-6, C-7, S-2, and S-3) with CC_{50} values close to 100 μM were categorized as having strong cytotoxicity and were therefore not considered for further antiviral evaluation. Consequently, 5 compounds S-4, C-5, S-10, S-11, and S-12 were selected for further analysis.

***In vitro* anti-SARS-CoV-2 viral activity**

Five compounds S-4, C-5, S-10, S-11, and S-12 were selected based on preliminary cytotoxicity results for further evaluation of their anti-SARS-CoV-2 activity. The IC_{50} values were determined from dose-response curves using nonlinear regression (4-parameter logistic model) in GraphPad Prism 8.3.0. as described in **Table 3**.

Table 3 Antiviral activities of the compounds.

Compounds	IC_{50} value	Categories	Selectivity index	Categories
	Mean ± SD (μM)	(a)*	(Mean ± SD)	(b)*
S-4	25.21 ± 5.38	Moderate activity	17.1 ± 6.24	Selective bioactive
C-5	5.623 ± 0.24	Good activity	161.3 ± 19.40	Selective bioactive
S-10	8.52 ± 0.28	Good activity	158.8 ± 25.93	Selective bioactive
S-11	19.48 ± 0.91	Good activity	111.9 ± 19.09	Selective bioactive
S-12	6.187 ± 0.41	Good activity	309.7 ± 41.82	Selective bioactive

Notes: *a) Criteria of IC50: 1 - 20 μM good activity, 20 - 100 μM moderate activity (Indrayanto *et al.* [46]). *b) Criteria of Selectivity Index >10 very safe, 10 - 3 moderate (Indrayanto *et al*. [46]).

Figure 2 shows the IC_{50} values of the compounds against SARS-CoV-2. According to the established classification criteria Batista *et al*., 2009 in Indrayanto *et al*. [46] compounds with IC_{50} values < 20 μM are considered to have strong antiviral activity. In this study, C-5 (5.62 ± 0.24 μM), S-12 (6.19 ± 0.41 μM), and S-10 (8.52 ± 0.28 μM) demonstrated the highest potency, whereas S-4 (25.21 ± 5.38 μM) was moderately active.

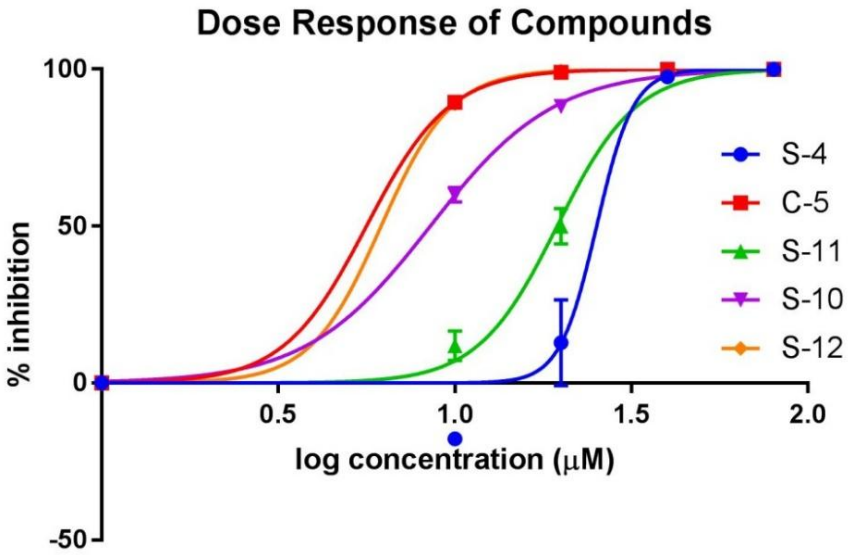

Figure 2 Dose-response curves of selected chalcone (C-5), chromene (S-10, S-11), and dihydropyrimidinone (S-4, S-12) derivatives showing antiviral activity against SARS-CoV-2 in Vero cells. The tested concentrations were 10, 20, 40, and 80 μM. Color codes: S-4 (blue), C-5 (red), S-11 (green), S-10 (purple), and S-12 (orange). Data are shown as mean ± SD. Each concentration was tested in triplicate.

Statistical analysis using one-way ANOVA followed by Tukey's post hoc test (**Table 3**) revealed significant differences among several compound pairs. Notably, compounds C-5, S-10, and S-12, which exhibited the lowest IC_{50} values, were statistically different from the other tested compounds ($p < 0.05$). Although there were no significant differences among C-5, S-10, and S-12 themselves, each showed significantly lower IC_{50} values compared to the remaining compounds.

Table 3 Pairwise IC_{50} comparison (one-way ANOVA followed by Tukey's post hoc test).

Comparison	Mean Diff.	95% CI	Significant	*p*-value
S-4 vs. S-10	14.66	7.77 to 21.55	Yes (**)	0.002
S-4 vs. S-12	16.95	10.06 to 23.84	Yes (***)	0.001
S-4 vs. C-5	17.63	10.74 to 24.52	Yes (***)	0.0008
C-5 vs. S-11	–14.63	–21.51 to –7.736	Yes (**)	0.002
S-10 vs. S-11	–11.65	–18.54 to –4.76	Yes (**)	0.0056
S-12 vs. S-11	13.94	7.05 to 20.83	Yes (**)	0.0025
C-5 vs. S-10	–2.973	–9.862 to 3.916	No	0.492
C-5 vs. S-12	–0.6836	–7.573 to 6.206	No	0.993
S-10 vs. S-12	2.289	–4.600 to 9.178	No	0.6869

Notes: *$p < 0.05$, **$p < 0.01$, ***$p < 0.001$.

The selectivity index (SI), defined as the ratio of CC_{50} to IC_{50}, indicates the margin of safety for each compound. It was used to evaluate the therapeutic potential. Based on the data in **Figure 3**, all tested

compounds had SI ≥ 10, with S-12 (SI = 309.7), C-5 (SI = 161.3), and S-10 (SI = 158.8) showing the most favorable profiles for further evaluation. In contrast, the moderate SI values for S-4 and S-11 (17.1 and 111.9, respectively) suggest that structural modifications are necessary to improve their efficacy and safety profiles.

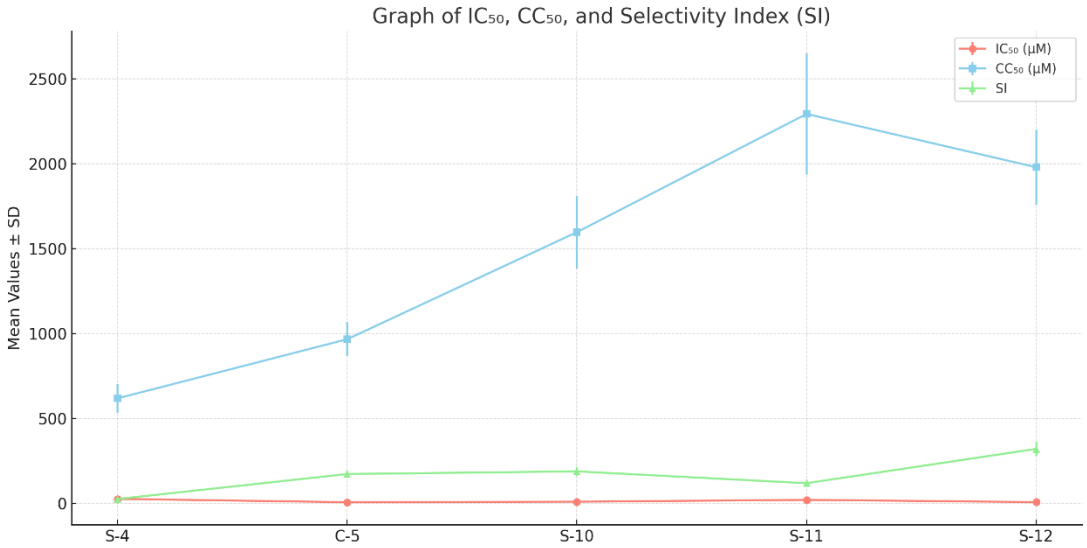

Figure 3 IC_{50}, CC_{50}, and Selectivity Index (SI) values (mean ± SD) of selected compounds. The IC_{50} values (red), represent the concentration required to inhibit 50% of SARS-CoV-2 viral activity in Vero cells, while the CC_{50} values (blue), represent the concentration at which 50% of the cells exhibit cytotoxicity. The selectivity index (SI) is the ratio of CC_{50} to IC_{50} (green), indicating the margin of safety for each compound.

Although direct comparisons with FDA-approved commercial antivirals such as remdesivir were not performed in this study, the IC_{50} values of C-5, S-10, and S-12 were found to fall within the low micromolar range. For contextual reference, previous studies have reported IC_{50} values of remdesivir between 0.77 and 1.65 μM in Vero E6 and human lung cells [47,48]. These comparisons are presented merely as background information and should not be interpreted as evidence of equivalent efficacy. Instead, the present findings highlight the preliminary antiviral potential of the tested compounds, indicating the need for further investigation and direct comparative studies with standard drugs such as remdesivir to clarify their relative effectiveness.

ADME characteristics of the compounds

To support further evaluation of the selected compounds, an *in silico* analysis of absorption, distribution, metabolism, and excretion (ADME) properties was conducted. This analysis aimed to estimate drug-likeness and potential pharmacokinetic behavior by applying Lipinski's rule of 5, as well as the Ghose and Veber criteria. The evaluated parameters included molecular weight (MW), number of hydrogen bond donors and acceptors, rotatable bonds, molecular refractivity (MR), topological polar surface area (TPSA), predicted octanol-water partition coefficient (WLOGP), and blood-brain barrier (BBB) permeability [49].

Table 5 ADME prediction analysis.

No.	Codes compounds	MW	#Heavy atoms	#Rotatable bonds	#H-bond acceptors	#H-bond donors	MR	TPSA	WLOGP	BBB	LD_{50}	Mut	SS ADME
1	C-1	223.27	17	3	1	1	70.65	43.09	3.06	Yes	3351.8	0.03	0.9444
2	S-2	246.33	17	2	1	2	79.09	73.22	0.98	No	694.7	0.67	0.9444
3	S-3	242.3	17	2	3	1	68.31	100.89	2.33	No	1103.5	0.98	0.9444
4	S-4	252.36	16	2	1	2	76.96	101.46	1.04	No	1250.9	0.68	0.9444

No.	Codes compounds	MW	#Heavy atoms	#Rotatable bonds	#H-bond acceptors	#H-bond donors	MR	TPSA	WLOGP	BBB	LD_{50}	Mut	SS ADME
5	C-5	450.51	33	6	4	1	132.94	100.44	6.45	No	561.5	0.66	0.9444
6	C6	282.36	20	5	1	2	86.05	87.21	2.94	No	1022.9	0.5	0.9444
7	C7	288.39	19	5	1	2	83.93	115.45	3	No	610.5	0.75	0.9444
8	S10	264.28	20	1	3	2	73.89	79.27	2.61	No	946.9	0.67	0.9444
9	S11	263.29	20	1	2	2	76.27	85.06	2.49	No	1144.6	0.76	0.9444
10	S12	260.29	19	4	3	2	77.78	67.43	0.79	No	936.7	0.33	0.9444
11	Nirmatrelvir	531.88	37	6	9	1	128.08	117.45	3.59	No	81.5	0.08	0.2222
12	Ritonavir	329.31	23	6	8	4	76.02	143.14	–1.65	No	824.2	0.25	0.7222
13	Remdesivir	720.94	50	22	7	4	197.82	202.26	5.60	No	331.12	0.10	0.4167
14	Ensitrelvir	602.58	42	14	12	4	150.43	213.36	2.21	No	921.9	0.11	0.3611
15	Favipiravir	613.79	45	14	7	4	182.62	118.03	1.63	No	2000.16	0.33	0.6667

Notes: MW = Molecular weight, MR = Molar refractivity, TPSA = Polar surface area, Log P = Water partition coefficient, BBB = Blood-Brain Barrier permeability, LD_{50} = 50% lethal-dose, Mut = Ames's mutagenicity, SS ADME = ADME Selection Score.

According to **Table 5**, all 5 compounds that passed *in vitro* screening (C-5, S-4, S-10, S-11, and S-12) fulfilled the general molecular weight requirement (MW < 500), which correlates with enhanced cellular permeability and oral bioavailability. Additionally, all compounds had TPSA values below 120 Å², indicating favorable potential for passive gastrointestinal absorption. The WLOGP values of most compounds also fell within the optimal range of –0.4 to 5.6, suggesting a balanced lipophilicity. However, compound C-5 exhibited a WLOGP value exceeding this threshold, indicating a risk of low solubility. Poor solubility can negatively impact drug absorption and bioavailability, especially for orally administered drugs [37,34].

Regarding BBB permeability, none of the compounds were predicted to cross the blood-brain barrier, which may be advantageous in avoiding central nervous system (CNS) side effects for drugs targeting respiratory viral infections. Toxicity risk was further assessed using the Selection Score (SS), which integrates ADME parameters and predicted toxicity. Compounds S-4, S-10, S-11, and S-12 demonstrated SS values closer to 1, indicating more favorable predicted safety and pharmacokinetic profiles than the other compounds [50,51].

Overall, while *in silico* ADME predictions suggested acceptable pharmacokinetic characteristics for 4 of the 5 selected compounds, it is important to note that these findings remain predictive. Experimental validation through solubility testing, permeability assays, and pharmacokinetic studies is necessary to confirm their drug-like behavior *in vivo* is necessary.

Therefore, S-10 and S-12 have high selectivity index values, favorable *in silico* ADMET profiles, and structurally simpler scaffolds, making them attractive candidates for further optimization. Unlike Remdesivir, which requires intravenous administration and intracellular activation, the tested compounds (S-10 and S-12) show potential for oral bioavailability and cost-effective synthesis, offering significant advantages for broad antiviral development, especially in low-resource settings.

The molecular docking analysis

The SARS-CoV-2 main protease (Mpro) is a cysteine protease derived from a polyprotein that forms a homodimer with catalytic residues His-41 and Cys-145 at the active site. Cys-145 functions as a nucleophile, while His-41 assists in proton transfer, making both essential for enzymatic cleavage [52,53]. The co-crystallized ligand X77, used as a docking reference, engages in van der Waals interactions and hydrogen bonds with key residues such as Ser-144, His-163, and Glu-166, along with a salt bridge with His-163 [54]. As summarized in **Table 6**, the docking results indicated that 4 candidate compounds (S-4, S-10, S-11, and S-12) interacted with key catalytic residues (Cys-145 and His-41). These interactions include hydrogen bonding, hydrophobic contacts, π – π stacking, and

electrostatic interactions, all of which are essential for inhibitory activity.

Importantly, the observed interactions with His-41 and Cys-145 are consistent with those reported for known SARS-CoV-2 protease inhibitor, suggesting potential biological relevance in enzyme inhibition [55,56]. Nevertheless, docking results represent predictive binding affinity and should be interpreted cautiously, as this approach does not account for protein flexibility, solvent effects, or pharmacokinetic properties. Therefore, the molecular docking data in this study are intended to complement and support the preliminary *in vitro* findings, rather than to provide definitive evidence of antiviral efficacy [57,58].

Tabel 6 Docking results of the compounds on Mpro.

Compound	Docking Score (kcal/mol)	H-Bond Residues	π bonds and Hydrophobic bonds Interactions	Catalytic Dyad (His-41/Cys-145)
X77 (native)	–83.532	Glu166; His163; Gly143	His41; Cys145; Met49; Leu141; Asn142; Met165	✔ His-41/ ✔ Cys-145
Lopinavir	–89.638	Glu166; Gln192; Pro168	His41; Cys145; Met49; Cys44; Met165	✔ His-41/ ✔ Cys-145
Remdesivir	–92.693	Glu166; Gln188; Arg188	His41; Cys145; Met49; Cys44; Asp187; Asn142	✔ His-41/ ✔ Cys-145
Ritonavir	–101.209	Glu166	His41; Pro168; Met49; Met165; Thr24 - 26; Leu167	✔ His-41/ ✔ Cys-145
Nirmatrelvir	–78.309	His163; Glu166; Gly143; Phe140; Ser144; Gln192	His41; Met49; Met165; Gln189; Pro168	✔ His-41/✗ Cys-145
Molnupiravir	–59.122	His163; Met165; Arg188; Cys145	Asp187; Met165	✗ His-41/ ✔ Cys-145
Favipiravir	–34.287	Glu166; His163; Phe140; Ser144; Cys145	Asn142; Leu141; Met165	✗ His-41/ ✔ Cys-145
Ensitrelvir	–72.11	His163; Glu166; Gly143; Ser144; Met49; Thr25	His41; Cys145; Met165; Asp187; Gln189	✔ His-41/ ✔ Cys-145
S-4	–33.723	Glu166; Gln189; Gln192; Arg188	His41; Asp187; Met165	✔ His-41/✗ Cys-145
S-10	–34.488	Asp187; Cys44	His41; Cys145; Met165; Met49; Arg188	✔ His-41/ ✔ Cys-145
S-11	–34.622	Asp187; Cys44	His41; Cys145; Met49; Cys44	✔ His-41/ ✔ Cys-145
S-12	–37.047	Asp187; His163	His41; Cys145; Met49; Glu166; Met165; Arg188	✔ His-41/ ✔ Cys-145

Molecular docking visualization

Chromene derivatives

Docking analysis revealed that S-10 and S-11 as shown in **Figure 4(A)** (yellow and red) closely resembled the orientation of the reference inhibitor X77, the original ligand of the main protease (PDB ID: 6W63, **Figure 4(B)**; magenta). Both compounds formed interactions with the catalytic residues His-41 and Cys-145. For S-10, the structure includes amino, hydroxyl, and phenyl groups, which facilitate hydrogen bonding and hydrophobic interactions. The hydroxyl and amino groups enhanced hydrogen bonding with the Mpro catalytic dyad, while the phenyl group established hydrophobic contacts within the S1 pocket of the Mpro active site. These combined interactions stabilized the binding orientation and improved antiviral potency [59].

Meanwhile, S-11, which contained diamino, phenyl, and carbonitrile groups, adopted a less favourable binding mode. The high polarity of diamino substituent increased hydrophilicity, thereby limiting hydrogen bond formation at the catalytic site and reducing membrane permeability, which in turn decreased intracellular accumulation. These molecular features are consistent with the biological data, where S-10 exhibited stronger antiviral activity (IC_{50} = 8.52 μM,

SI = 158.8) compared to S-11 (IC_{50} = 19.48 μM, SI = 111.9).

DHPM derivatives

Docking analysis revealed that S-12 (**Figure 4(A)**; light blue color) closely resembled the binding orientation of the reference inhibitor X77, the original ligand of Mpro (PDB ID: 6W63, **Figure 4(B)**; magenta). The compound exhibited strong interactions within the active site by forming hydrogen bonds with the catalytic residues His-41 and Cys-145, π – π stacking with His-41, and a salt bridge with His-163. These multiple interactions stabilized the ligand within the pocket. In addition, the carbonyl and phenyl groups improved binding stability, while the carboxylate group enhanced aqueous solubility and electrostatic stabilization, further supporting ligand bioavailability and target engagement.

In comparison, S-4 (**Figure 4(A)**; purple color) adopted a less favorable orientation relative to X77 (**Figure 4(B)**). It interacted with His-41 primarily through van der Waals forces, which were insufficient to secure strong binding. Structurally, S-4 contained thiophene, methyl, and thioxo groups that increased lipophilicity but provided limited opportunities for hydrogen bonding with the catalytic residues, leading to weaker stabilization in the active site [59].

These docking observations are in line with the biological results, where S-12 demonstrated the strongest antiviral effect among the DHPM derivatives (IC_{50} = 6.187 μM, SI = 309.7), while S-4 showed weaker activity (IC_{50} = 25.21 μM, SI = 17.1). Overall, these results emphasize that polar functional groups capable of hydrogen bonding (e.g., hydroxyl, amino, carboxyl) are more favorable than lipophilic substituents in achieving potent inhibition of SARS-CoV-2 Mpro

.

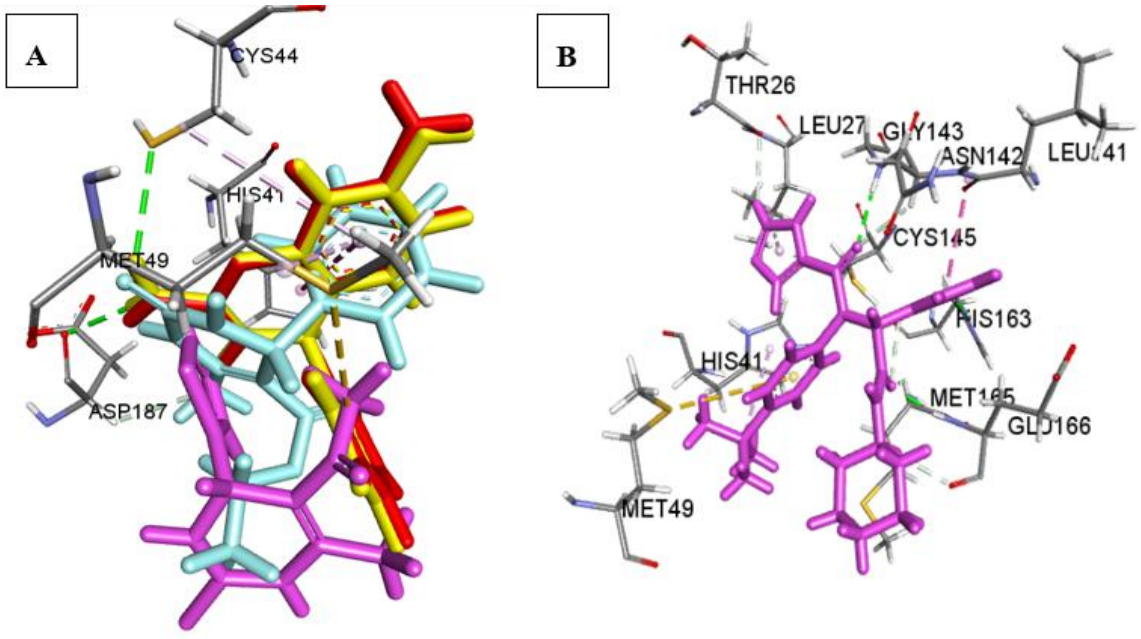

Figure 4 Molecular docking visualization of selected compounds with SARS-CoV-2 main protease (Mpro, PDB ID: 6W63). (A) Superimposed docking poses of candidate compounds: S-10 (yellow), S-11 (red), S-12 (light blue), and S-4 (purple). (B) Binding interaction of the co-crystallized ligand X77 (magenta) at the Mpro active site (visualized using the Biovia Discovery Studio).

Docking simulations in this study included the native ligand X77, FDA-approved antivirals (e.g., Remdesivir, Ritonavir, Lopinavir, Nirmatrelvir), and the tested compounds (S-4, S-10, S-11, S-12). As shown in **Table 6**, the reference inhibitors consistently interacted with His-41 and Cys-145, confirming the catalytic dyad as a critical binding region. Among the candidate compounds, S-12 displayed the most favorable docking score and binding pose, showing interaction patterns comparable to X77 and several reference antivirals

[60,61]. S-10 also engaged in hydrogen bonding and hydrophobic contacts with the catalytic residues, whereas S-4 and S-11 showed weaker scores and less optimal orientations. These findings suggest that S-12 and S-10 may possess favorable binding modes at the Mpro active site; however, it should be emphasized that docking provides only predictive interaction patterns [62] and does not account for protein flexibility or solvent dynamics, so further validation is required.

Conclusions

This study identified 2 lead compounds, S-12 and S-10, from DHPM, chromene, and chalcone scaffolds, which exhibited potent *in vitro* antiviral activity against a locally isolated SARS-CoV-2 strain, with low cytotoxicity, high selectivity index (>100), and favorable drug-like properties. *In silico* analyses further supported their oral bioavailability and the absence of major toxicity alerts. Although, their IC_{50} values were higher than those of approved antivirals such as Remdesivir, based on literature reports, but their simpler structures, lower cytotoxicity, and synthetic accessibility suggest practical advantages as early-stage candidates. A key limitation, however, is the absence of direct *in vitro* comparison with clinically used antivirals, which would provide stronger context for potency evaluation. Molecular docking revealed stable interactions with the catalytic residues His-41 and Cys-145 of Mpro, supporting their relevance as potential protease inhibitors, though such predictions remain preliminary. Overall, these findings highlight S-12 and S-10 as promising scaffolds that indicate the need for further *in vivo* validation, pharmacokinetic studies, structural optimization, and direct benchmarking against reference antivirals to advance their development as region-specific anti-SARS-CoV-2 agents.

Acknowledgements

This Research is financially supported by Indonesian Ministry of Higher Education through Research Funds (DRTPM) 2023 in platform Doctoral Research Grant for 1 year study based on No. 114/E5/PG.02.00.PL/2023; UN3.LPPM/PT.01.03/2023 and fully support of BIOME as well as ITD Universitas Airlangga.

Declaration of generative AI in scientific writing

Generative AI tools (e.g., ChatGPT by OpenAI, Grammarly) were used exclusively to enhance the clarity, grammar, and readability of the manuscript. All scientific content, including study design, data analysis, interpretation, and conclusions, was entirely developed and verified by the authors. The use of AI was conducted under full human oversight, and the authors assume complete responsibility for the integrity and accuracy of the work. No AI tool is listed as an author or co-author.

Credit author statement

Dinar Adriaty: Writing - Original Draft preparation, Conceptualization, Methodology, Investigation, Formal Analysis, Visualization, Software; **Hery Suwito:** Resources, Conceptualization; Data curation, Writing - Reviewing and Editing. **Ni Nyoman Tri Puspaningsih:** Resources; Funding acquisition, Writing - Reviewing and Editing; **Adita Ayu Permanasari:** Supervision, Validation; **Aldise Mareta Nastri:** Supervision, Validation; **Kazufumi Shimizui:** Resources, Writing - Reviewing and Editing.

References

[1] H Zhu, L Wei and P Niu. The novel coronavirus outbreak in Wuhan, China. *Global Health Research and Policy* 2020; **5(1)**, 6.

[2] B Hu, H Guo, P Zhou and ZL Shi. Characteristics of SARS-CoV-2 and COVID-19. *Nature Reviews Microbiology* 2021; **19(3)**, 141154.

[3] A Gori, F Fama and C Genovese. *Coronavirus disease 19 (COVID-19)*. *In*: MCB Raviglione, F Tediosi, S Villa, N Casamitjana and A Plasència (Eds.). Global Health Essentials. Springer, Cham, Switzerland, 2023, p. 137-142.

[4] I Polatoğlu, T Oncu-Oner, I Dalman and S Ozdogan. COVID-19 in early 2023: Structure, replication mechanism, variants of SARS-CoV-2, diagnostic tests, and vaccine & drug development studies. *MedComm* 2023; **4(2)**, e228.

[5] Purwati, A Miatmoko, Nasronudin, E Hendrianto, D Karsari, A Dinaryanti, N Ertanti, IS Ihsan, DS Purnama, TP Asmarawati, E Marfiani, Yulistiani, AN Rosyid, PA Wulaningrum, HW Setiawan, I Siswanto and NNT Puspaningsih. An *in vitro* study of dual drug combinations of anti-viral agents, antibiotics, and/or hydroxychloroquine

against the SARS-CoV-2 virus isolated from hospitalized patients in Surabaya, Indonesia. *PLoS One* 2021; **16(6)**, e0252302.

[6] H Zhou, WJ Ni, W Huang, Z Wang, M Cai and YC Sun. Advances in pathogenesis, progression, potential targets and targeted therapeutic strategies in SARS-CoV-2-induced COVID-19. *Frontiers in Immunology* 2022; **13**, 834942.

[7] JD Rigg. *The Sustainable Development Goals (SDGS)*. *In*: The companion to development studies. Routledge, Oxfordshire, 2024, p. 253-257.

[8] EL Berg. The future of phenotypic drug discovery. *Cell Chemical Biology* 2021; **28(3)**, 424-430.

[9] F Vincent, A Nueda, J Lee, M Schenone, M Prunotto and M Mercola. Phenotypic drug discovery: Recent successes, lessons learned and new directions. *Nature Reviews Drug Discovery* 2023; **21(12)**, 899-914.

[10] S Wang, Z Wang, L Fang, Y Lv and G Du. Advances of the target-based and phenotypic screenings and strategies in drug discovery. *Internatioal Journal of Drug Discovery and Pharmacology* 2022; **1(1)**, 5-11.

[11] SE Rhabori, AE Aissouq, S Chtita and F Khalil. QSAR, molecular docking and ADMET studies of quinoline, isoquinoline and quinazoline derivatives against *Plasmodium falciparum* malaria. *Structural Chemistry* 2023; **34(2)**, 585-603.

[12] AM Andrianov, YV Kornoushenko, AD Karpenko, IP Bosko and AV Tuzikov. Computational discovery of small drug-like compounds as potential inhibitors of SARS-CoV-2 main protease. *Journal of Biomolecular Structure and Dynamics* 2021; **39(15)**, 5779-5791.

[13] I Amalina, NNT Puspaningsih and H Suwito. *In silico* analysis of pyrimidine derivatives as potential antibacterial agents. *In*: Proceedings of the International Conference on Advanced Technology and Multidiscipline, Surabaya, Indonesia. 2023, p. 50004.

[14] LHS Matos, FT Masson, LA Simeoni and M Homem-de-Mello. Biological activity of dihydropyrimidinone (DHPM) derivatives: A systematic review. *European Journal of Medical Chemistry* 2018; **143**, 1779-1789.

[15] AN Kristanti, H Suwito, NS Aminah, KU Haq, HD Hardiyanti, H Anggraeni, N Faiza, RS Anto and S Muharromah. Synthesis of some chalcone derivatives, *in vitro* and *in silico* toxicity evaluation. *Rasayan Journal of Chemistry* 2020; **13(1)**, 654-662.

[16] A Chaudhary, K Singh, N Verma, S Kumar, D Kumar and PP Sharma. Chromenes - A novel class of heterocyclic compounds: Recent advancements and future directions. *Mini Reviews in Medicinal Chemistry* 2022; **22(21)**, 2736-2751.

[17] V Raj and J Lee. 2H/4H-chromenes - A versatile biologically attractive scaffold. *Frontiers in Chemistry* 2020; **8**, 623.

[18] S Khasimbi, F Ali, K Manda, A Sharma, G Chauhan and S Wakode. Dihydropyrimidinones scaffold as a promising nucleus for synthetic profile and various therapeutic targets: A review. *Current Organic Synthesis* 2020; **18(3)**, 270-293.

[19] BT Dharmapalan, R Biswas, S Sankaran, B Venkidasamy, M Thiruvengadam, G George, M Rebezov, G Zengin, M Gallo, D Montesano, D Naviglio and MA Shariati. Inhibitory potential of chromene derivatives on structural and non-structural proteins of dengue virus. *Viruses* 2022; **14(12)**, 2656.

[20] SM Villa, J Heckman and D Bandyopadhyay. Medicinally privileged natural chalcones: Abundance, mechanisms of action, and clinical trials. *International Journal of Molecular Sciences* 2024; **25(17)**, 9623.

[21] SY Ham, H Jeong, J Jung, ES Kim, KU Park, HB Kim, JS Park and KH Song. Performance of STANDARD™ M10 SARS-CoV-2 assay for the diagnosis of COVID-19 from a nasopharyngeal swab. *Infection and Chemotherapy* 2022; **54(2)**, 360-363.

[22] Y Shu and J McCauley. GISAID: Global initiative on sharing all influenza data – from vision to reality. *Euro Surveillance* 2017; **22(13)**, 30494.

[23] K Rahardjo, AM Nastri, JR Dewantari, RR Prasetya, J Wahyuhadi, G Soegiarto, L Wulandari, RA Setyoningrum, R Yudhawati, YK Shimizu, M Nishimura, Y Mori, Soetjipto, K Shimizu and MI Lusida. *GISAID: EpiCoV database*. 2020. https://www.epicov.org/epi3/frontend#3280a8.

[24] M Brandolini, F Taddei, MM Marino, L Grumiro, A Scalcione, ME Turba, F Gentilini, M Fantini, S

Zannoli, G Dirani and V Sambri. Correlating qRT-PCR, dPCR and viral titration for the identification and quantification of SARS-CoV-2: A new approach for infection management. *Viruses* 2021; **13(6)**, 1022.

[25] G McDonnell and DM Hansen. *Block's disinfection, sterilization and preservation*. 6th eds. Lippincott Williams and Wilkins, Philadelphia, 2020.

[26] AA Permanasari, C Aoki-Utsubo, TS Wahyuni, L Tumewu, M Adianti, A Widyawaruyanti, H Hotta and AF Hafid. An *in vitro* study of an *Artocarpus heterophyllus* substance as a hepatitis C antiviral and its combination with current anti-HCV drugs. *BMC Complementary Medicine and Therapies* 2021; **21(1)**, 260.

[27] R Ramadhan, K Ul-Haq, P Phuwapraisirisan, FA Puspitasari and H Suwito. α-glucosidase inhibitory activities and antioxidant properties of depsidone from *Garcinia parvifolia*. *Rasayan Journal of Chemistry* 2023; **16(3)**, 1811-1817.

[28] H Suwito, R Ramadhan, A Abdulloh and KU Haq. Synthesis of dihydrotetrazolopyrimidine derivatives as anticancer agents and inhibitor of α-glucosidase. *Rasayan Journal of Chemistry* 2023; **16(1)**, 147-158.

[29] A Purniawan, MI Lusida, RW Pujiyanto, AM Nastri, AA Permanasari, AAH Harsono, NH Oktavia, ST Wicaksono, JR Dewantari, RR Prasetya, K Rahardjo, M Nishimura, Y Mori and K Shimizu. Synthesis and assessment of copper-based nanoparticles as a surface coating agent for antiviral properties against SARS-CoV-2. *Scientific Reports* 2022; **12(1)**, 4835.

[30] VNT La, S Nicholson, A Haneef, L Kang and DDL Minh. Inclusion of control data in fits to concentration-response curves improves estimates of half-maximal concentrations. *Journal of Medical Chemistry* 202; **66(18)**, 12751-12761.

[31] L Grumiro, M Brandolini, G Gatti, A Scalcione, F Taddei, G Dirani, A Mancini, A Denicolò, M Manera, S Zannoli, MM Marino, M Morotti, V Arfilli, A Battisti, M Cricca and V Sambri. Evaluation of STANDARD™ M10 SARS-CoV-2, a novel cartridge-based real-time PCR assay for the rapid identification of severe acute respiratory syndrome coronavirus 2. *Applied Microbiology* 2022; **2(4)**, 873-881.

[32] A Daina, O Michielin and V Zoete. SwissADME: A free web tool to evaluate pharmacokinetics, drug-likeness and medicinal chemistry friendliness of small molecules. *Scientific Reports* 2017; **7**, 42717.

[33] S Abu-Melha, MM Edrees, MA Said, SM Riyadh, NS Al-Kaff and SM Gomha. Potential COVID-19 drug candidates based on diazinyl-thiazol-imine moieties: Synthesis and greener pastures biological study. *Molecules* 2022; **27(2)**, 488.

[34] CA Lipinski, F Lombardo, BW Dominy and PJ Feeney. Experimental and computational approaches to estimate solubility and permeability in drug discovery and development settings. *Advanced Drug Delivery Reviews* 2001; **46(1-3)**, 3-25.

[35] R Yadav, M Imran, P Dhamija, DK Chaurasia and S Handu. Virtual screening, ADMET prediction and dynamics simulation of potential compounds targeting the main protease of SARS-CoV-2. *Journal of Biomolecular Structure and Dynamics* 2021; **39(17)**, 6617-6632.

[36] L Vegosen and TM Martin. An automated framework for compiling and integrating chemical hazard data. *Clean Technologies and Environmental Policy* 2020; **22(2)**, 441-458.

[37] TM Martin. User's Guide for T.E.S.T. (Toxicity Estimation Software Tool) Version 5.1. 2020, Available at: https://www.epa.gov/chemical-research/toxicity-estimation-software-tool-test, accessed May 2025.

[38] JA Maier, C Martinez, K Kasavajhala, L Wickstrom, KE Hauser and C Simmerling. ff14SB: Improving the accuracy of protein side chain and backbone parameters from ff99SB. *Journal of Chemical Theory and Computation* 2015; **11(8)**, 3696-3713.

[39] S Kumar and S Kumar. *Molecular docking: A structure-based approach for drug repurposing*. *In*: K Roy (Ed.). *In silico* drug design. Academic Press, Massachusetts, 2019, p. 161-189.

[40] MS Coumar. *Molecular docking for computer-aided drug design: Fundamentals, Techniques, Resources and Applications*. Academic Press, Massachusetts, 2021.

[41] WJ Allen, TE Balius, S Mukherjee, SR Brozell,

DT Moustakas, PT Lang, DA Case, ID Kuntz and RC Rizzo. DOCK 6: Impact of new features and current docking performance. *Journal of Computational Chemistry* 2016; **36(15)**, 1132-1156.

[42] S Khasimbi, F Ali, K Manda, A Sharma, G Chauhan and S Wakode. Dihydropyrimidinones scaffold as a promising nucleus for synthetic profile and various therapeutic targets: A review. *Current Organic Synthesis* 2021; **18(3)**, 270-293.

[43] P Pérez-Ramos, G Biniari, RG Soengas, H Rodríguez-Solla and C Simal. Visible-light photocatalysis for sustainable chromene synthesis and functionalization. *Chemistry* 2025; **31(29)**, e202500283.

[44] WW Mar, KU Haq, RA Rusdipoetra, RPFC Samiadji, A Rohman, NNT Puspaningsih and H Suwito. Anticancer activity through inhibition of $BCL6^{BTB}$ of chalcone - Thiourea hybrid compounds: A molecular docking study. *AIP Conference Proceedings* 2023; **2679(1)**, 50009.

[45] I Amalina, NNT Puspaningsih and H Suwito. *In silico* analysis of pyrimidine derivatives as potential antibacterial agents. *AIP Conference Proceedings* 2023; **2536**, 50004.

[46] G Indrayanto, GS Putra and F Suhud. Validation of *in-vitro* bioassay methods: Application in herbal drug research. *Profiles of Drug Substances, Excipients and Related Methodology* 2021; **46**, 273-307.

[47] AJ Pruijssers, AJ Pruijssers, AS George, A Schäfer, SR Leist, LE Gralinksi, KH Dinnon, BL Yount, ML Agostini, LJ Stevens, JD Chappell, X Lu, TM Hughes, K Gully, DR Martinez, AJ Brown, RL Graham, JK Perry, VD Pont, J Pitts, …, TP Sheahan. Remdesivir inhibits SARS-CoV-2 in human lung cells and chimeric SARS-CoV expressing the SARS-CoV-2 RNA polymerase in mice. *Cell Reports* 2020; **32(3)**, 107940.

[48] M Wang, R Cao, L Zhang, X Yang, J Liu, M Xu, Z Shi, Z Hu, W Zhong and G Xiao. Remdesivir and chloroquine effectively inhibit the recently emerged novel coronavirus (2019-nCoV) *in vitro*. *Cell Research* 2020; **30(3)**, 269-271.

[49] B Morak-Młodawska, M Jeleń, E Martula and R Korlacki. Study of lipophilicity and ADME properties of 1,9-diazaphenothiazines with anticancer action. *International Journal of Molecular Sciences* 2023; **24(8)**, 6970.

[50] LM Castro-González, JR Alvarez-Idaboy and A Galano. Computationally designed sesamol derivatives proposed as potent antioxidants. *ACS Omega* 2020; **5(16)**, 9566-9575.

[51] A Pérez-González, R Castañeda-Arriaga, EG Guzmán-López, LF Hernández-Ayala and A Galano. Chalcone derivatives with a high potential as multifunctional antioxidant neuroprotectors. *ACS Omega* 2022; **7(43)**, 38254-38268.

[52] A Fischer, M Sellner, S Neranjan, M Smieško and MA Lill. Potential inhibitors for novel coronavirus protease identified by virtual screening of 606 million compounds. *International Journal of Molecular Sciences* 2020; **21(10)**, 3626.

[53] Z Jin, X Du, Y Xu, Y Deng, M Liu, Y Zhao, B Zhang, X Li, L Zhang, C Peng, Y Duan, J Yu, L Wang, K Yang, F Liu, R Jiang, X Yang, T You, X Liu, …, H Yang. Structure of M^{pro} from SARS-CoV-2 and discovery of its inhibitors. *Nature* 2020; **582**, 289-293.

[54] S Guo, H Xie, Y Lei, B Liu, L Zhang, Y Xu and Z Zuo. Discovery of novel inhibitors against main protease (Mpro) of SARS-CoV-2 via virtual screening and biochemical evaluation. *Bioorganic Chemisty* 2021; **110**, 104767.

[55] B Chatterjee and SS Thakur. Remdesivir and its combination with repurposed drugs as COVID-19 therapeutics. *Frontiers in Immunology* 2022; **13**, 830990.

[56] M Prajapat, Sarma, N Shekhar, P Avti, S Sinha, H Kaur, S Kumar, A Bhattacharyya, H Kumar, S Bansal and B Medhi. Drug targets for corona virus: A systematic review. *Indian Journal of Pharmacology* 2020; **52(1)**, 56-65.

[57] A Shirali, V Stebliankin, U Karki, J Shi, P Chapagain and G Narasimhan. A comprehensive survey of scoring functions for protein docking models. *BMC Bioinformatics* 2025; **26**, 25.

[58] A Harmalkar and JJ Gray. Advances to tackle backbone flexibility in protein docking. *Current Opinion in Structural Biology* 2021; **67**, 178-186.

[59] GL Patrick. *An introduction to medicinal chemistry*. 7th eds. Oxford University Press, Oxford, 2023.

[60] M Hariono, P Hariyono, R Dwiastuti, W Setyani,

M Yusuf, N Salin and H Wahab. Potential SARS-CoV-2 3CLpro inhibitors from chromene, flavonoid and hydroxamic acid compound based on FRET assay, docking and pharmacophore studies. *Results in Chemistry* 2021; **3**, 100195.

[61] S Gorai, V Junghare, K Kundu, S Gharui, M Kumar, BS Patro, SK Nayak, S Hazra and S Mula. Synthesis of dihydrobenzofuro[3,2-b]chromenes as potential 3CLpro inhibitors of SARS-CoV-2: A molecular docking and molecular dynamics study. *ChemMedChem* 2022; **17(8)**, e202100782.

[62] LH Al-Wahaibi, AM Elshamsy, TFS Ali, BGM Youssif, S Bräse, M Abdel-Aziz and NA El-Koussi. Design and synthesis of new dihydropyrimidine/sulphonamide hybrids as promising anti-inflammatory agents via dual mPGES-1/5-LOX inhibition. *Frontiers in Chemistry* 2024; **12**, 1387923.